Xia *et al. Satell Navig* (2021) 2:8
https://doi.org/10.1186/s43020-021-00035-1

Satellite Navigation
https://satellite-navigation.springeropen.com/

ORIGINAL ARTICLE Open Access

First results of BDS positioning for LBS applications in the UK

Yan Xia[1,2,3], Xiaolin Meng[4], Yusong Yang[5], Shuguo Pan[1,2*], Qing Zhao[6] and Wang Gao[1,2]

Abstract

The last satellite of BeiDou Navigation Satellite System with Global Coverage (BDS-3) constellation was successfully launched on June 23rd, 2020, and the entire system began to provide Positioning, Navigation, and Timing (PNT) services worldwide. We evaluated the performance of location services using BDS with a smartphone that can track the Global Navigation Satellite System (GNSS) satellites in Nottingham, UK. The static and kinematic experiments were conducted in an open meadow and a lakeside route covered by trees, respectively. Experimental results show that BDS has good visibility, and its overall signal carrier-to-noise density ratio (C/N_0) is comparable to that of Global Positioning System (GPS). The average C/N_0 of BDS-3 satellites with elevation angles above 45° on B1 band is the highest among all systems, reaching 40.0 dB·Hz. The noise level of the BDS pseudorange measurements is within 0.5 m, and it has a good consistency among satellites. In the static experiment, the standard deviations of BDS positioning in the east, north and up directions are 1.09, 1.16, and 3.02 m, respectively, and the R95 value of the horizontal position is 2.88 m. In harsh environments, the number of BDS satellites tracked by the smartphone is susceptible to environmental factors. The bias Root Mean Squares (RMS) in the three directions of the whole kinematic positioning are 6.83, 6.68, 11.67 m, in which the positioning bias RMS values in a semi-open environment are only 2.81, 1.11, 3.29 m. Furthermore, the inclusion of BDS in multiple GNSS systems can significantly improve the positioning precision. This study intends to provide a reference for the further improvements of BDS global PNT services, particularly for Location-Based Services (LBS).

Keywords: BDS, Android smartphone, Observation quality, LBS, UK

Introduction

Since Google announced in 2016 that it would make Global Navigation Satellite System (GNSS) raw observations available to the mobile devices with Android 7 and above, there has been an upsurge in studying GNSS positioning with a smartphone. The latest GNSS market reports (GSA 2019) show that smartphones contributed 1.5 billion units of the 1.8 billion GNSS receivers shipped worldwide in 2019, which indicates smartphones remain the most popular platform to support mobile Location-Based Services (LBS). The research on the theory and algorithm of the smartphone positioning has become one of the most popular topics in the GNSS field. Researchers have studied the positioning performance of Single Point Positioning (SPP), Real-Time Kinematic (RTK), and Precise Point Positioning (PPP) using GNSS observations collected by a variety of smartphones and developed some new algorithms (Zhang et al. 2018, 2019a; Odolinski and Teunissen 2019; Banville et al. 2019). Some derivative fields such as GNSS scenario recognition (Gao and Groves 2018; Xia et al. 2020) and mobile multi-source fusion positioning (Niu et al. 2019; Zhu et al. 2019) have also made considerable progress during this period. In 2018 Xiaomi released the world's first dual-frequency, namely Global Positioning System (GPS) L1/L5, Galileo navigation satellite system (Galileo) E1/E5a and Quasi-Zenith Satellite System (QZSS) L1/L5, GNSS smartphone called Xiaomi Mi 8, pushing the smartphone positioning research to a new culmination. The evolution

*Correspondence: psg@seu.edu.cn
[1] School of Instrument Science and Engineering, Southeast University, Nanjing 210096, China
Full list of author information is available at the end of the article

of multi-system and multi-frequency smartphone GNSS chipsets makes it possible for mobile users to obtain precise positioning results. At present, the horizontal accuracy of smartphone GNSS positioning is generally in the range of meter to sub-meter, including in urban environments (Liu et al. 2019; Fortunato et al. 2019; Chen et al. 2019). Some researchers claimed to achieve decimeter-level accuracy of PPP or RTK positioning (Gill et al. 2017; Zhang et al. 2019a). Banville et al. (2019) verified that static PPP positioning accuracy at centimeter level was achievable in a good observation condition and by virtue of the precise ionospheric corrections derived from a regional network of stations. Wanninger and Heßelbarth (2020) calibrated the antenna phase center for a Huawei P30 mobile phone and obtained short baseline RTK accuracy at centimeter level after fixing ambiguities using GPS L1 carrier phase measurements. Although the low gain and poor multipath mitigation of the GNSS antennas in smartphones limit the positioning accuracy, continuous hardware and software advancements make the positioning performance with smartphones getting closer to that of professional receivers.

Another crucial factor that impacts the rapid development of smartphone high-precision positioning is the modernization of GNSS, especially the emergence of new systems and new signals. The most notable system is Chinese BeiDou navigation satellite System (BDS). On June 23, 2020, the last satellite of the third generation BeiDou navigation satellite System (BDS-3) was successfully launched, marking the complete deployment of BDS global constellation. The completion of the BDS constellation extends the Positioning, Navigation, and Timing (PNT) services from the Asia–Pacific region to the rest of the world. BDS-3 is currently composed of 30 satellites, including 3 GEostationary Orbit (GEO) satellites, 24 Medium Earth Orbit (MEO) satellites and 3 Inclined Geosynchronous Orbit (IGSO) satellites. The new system retains the B1I and B3I signals of BeiDou navigation satellite (regional) System (BDS-2) and replaces B2I with B2b on the same frequency. Meanwhile, BDS-3 introduces two new signals, B1C/B2a, which are compatible with GPS L1/L5 and Galileo E1/E5a (Lu et al. 2019). Since the first two BDS-3 satellites were launched on November 5, 2017, researchers have conducted a lot of research on the new generation of navigation satellite system, including satellite visibility (Wang et al. 2019b), orbit determination (Wang et al. 2019a; Xie et al. 2019), error correction (Gu et al. 2020; Wang et al. 2020; Zhang et al. 2020), observation quality and positioning performance (Xie et al. 2018; Zhang et al. 2019b; Lv et al. 2020; Shi et al. 2020). Compared with BDS-2, BDS-3 has some significant improvements in clock stability, orbit accuracy, signal strength and pseudorange observation quality. The phase noise level of BDS-3 is comparable to that of BDS-2, GPS, and Galileo satellites (Zhang et al. 2019b). Besides, Beidou-3 shows superiority in system coverage, spatial signal accuracy, availability, and continuity (Guo et al. 2019; Yang et al. 2019, 2020). The rapid development of BDS enables global users to obtain accurate real-time location information with geodetic receivers or low-cost GNSS devices.

Nowadays, many domestic mainstream Android smartphones in China support BDS. Several overseas products such as Samsung and Google Pixel series can also receive BDS satellite signals. However, much attention has been paid to GPS-led mobile positioning, but little to BDS. Liu et al. (2019) and Chen et al. (2019) incorporated smartphone BDS observations in multi-system SPP and real-time PPP experiments, respectively. Wang et al. (2016), and Odolinski and Teunissen (2019) studied smartphone RTK positioning performance under different scenarios using multi-system observations including BDS. But very few research are on BDS-only positioning for LBS applications, especially outside the Asia–Pacific region. In addition, constrained by the previous system construction and the observation conditions for BDS-3, the results of some researches are inconclusive and even contradictory. BDS-3 global service needs to be investigated thoroughly from the perspective of positioning (Shi et al. 2020). From the above and with the completion of BDS, it is necessary to evaluate its capability in the smartphone positioning, including BDS alone and its integration with other GNSS constellations, so as to provide a reference for the further improvements in BDS global PNT services. Additionally, the 5G communication and positioning technology is booming, and smartphones are the ideal platforms of mobile networks. The research on BDS mobile location services also has a certain significance for promoting the integration of 5G and BDS on smartphones (Liu et al. 2020).

This article is the first to conduct a systematic evaluation of the smartphone BDS positioning performance outside the Asia–Pacific region, in Nottingham of the UK, since it's fully operational. Much attention is paid to how BDS performs in harsh environments. The structure of the article is as follows. Firstly, the satellite visibility and Geometric Dilution of Precision (GDOP) distribution of BDS constellation are analyzed, especially in the UK area. Secondly, we introduce the experimental design and data collection process. Thirdly, the quality of the smartphone BDS observations is assessed, including the carrier-to-noise density ratio and pseudorange measurement noise. Fourthly, we analyze the performances of smartphone BDS single point positioning in a static and open environment and a kinematic complex environment. The above experimental results are compared with those of other GNSS. Finally, we summarize our research findings.

BDS satellite visibility

The introduction of BDS-3 has greatly improved the service scope of BDS, and the number of satellites in orbit is 46 (i.e., 16 BDS-2 satellites and 30 BDS-3 satellites). From a global service perspective, the new system with 27 MEO satellites makes a considerable number of satellites visible to users. We employed the precise satellite orbit product of July 23, 2020 provided by German Research Centre for Geosciences (GFZ) to draw the 24-h ground tracks of BDS satellites, as shown in Fig. 1a, which contains 43 BDS satellites (no C18, C59 and C61). It can be seen that BDS MEO satellites cover most global areas except the polar regions and are densely distributed. Figure 1b depicts the nominal sky plot of the satellites at the static data collection site in Nottingham, central England. As many as 38 BDS satellites were visible in one day. In addition to all the existing 27 MEO satellites, 10 IGSO satellites and 1 GEO satellite (C05) were observed. However, due to the 55° inclination of MEO and IGSO satellite orbits, it is difficult for BDS satellites to cover most of the northern sky of the site, which limits the PNT services of BDS in higher latitudes (Meng et al. 2004). In the future, this situation can be improved by increasing the inclination of IGSO satellites (Yang et al. 2020).

For a more intuitive view of the instantaneous number of visible BDS satellites on the Earth, we divided the Earth surface into 5° × 2° grid cells and calculated the nominal number of visible satellites with elevation angles above 5° in each grid cell. The satellite visibility maps from the visual angle of Britain at GPS time 15:00:00, 16:00:00 and 17:00:00 are shown in Fig. 2. As can be seen from the figure, the number of visible BDS satellites with elevation angles above 5° in the UK was from 9 to 15 during the two-hour period. Globally, at least 6 satellites were observed, and the maximum number of visible satellites reached 30. In general, the Eastern Hemisphere had better satellite visibility than the Western Hemisphere due to the presence of IGSO and GEO satellites.

We calculated the nominal number of the visible satellites for BDS, GPS, Galileo and GLObal Navigation Satellite System (GLONASS) in the UK territory with a grid cell of 0.5° × 0.5°, and the elevation cutoff angle 5°, as shown in Fig. 3. One can see that BDS has the best satellite visibility, followed by GPS. The maximum of 16 BDS satellites can be observed over the UK territory.

Furthermore, we calculated the GDOP values for the BDS satellites at the above three moments using the same grid division and the same elevation cutoff angle. Figure 4 illustrates the GDOP distribution maps. The nominal GDOP values in the entire UK territory do not exceed 2, which is very satisfactory. Moreover, the GDOP values worldwide are within 3. Like the satellite visibility, the GDOP values in the Eastern Hemisphere are mostly lower than those in the Western Hemisphere.

For the UK area, Fig. 5 shows the distribution of the GDOP values for BDS, GPS, Galileo and GLONASS. In general, the nominal spatial geometric distribution of BDS satellites is also the most ideal with the maximum GDOP less than 2.2, which is consistent with the results in Fig. 4. The above results suggest BDS is favorable for the location-based services on a global scale. In the next step, we will use the measured GNSS data with a smartphone to evaluate BDS ranging precision and positioning performance in the UK territory.

GNSS data collection

Our experiments were conducted in the local afternoon of July 23, 2020 in Wollaton Park in Nottingham, UK. A Huawei Mate 20 smartphone was used to collect the static and kinematic observations of BDS/GPS/Galileo/

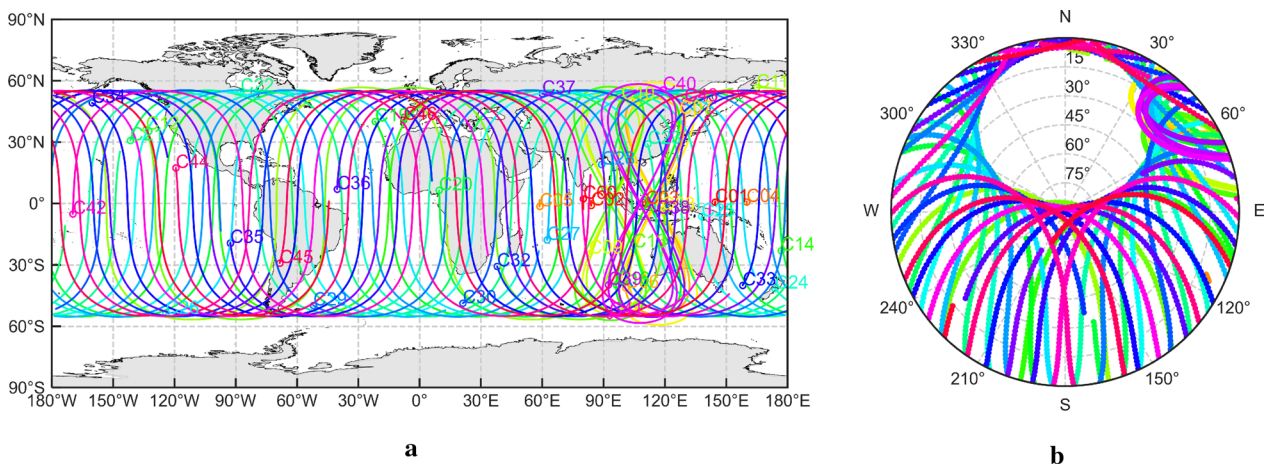

Fig. 1 **a** Ground tracks of BDS satellites and **b** the sky plot at an observation site in Nottingham, UK on July 23, 2020

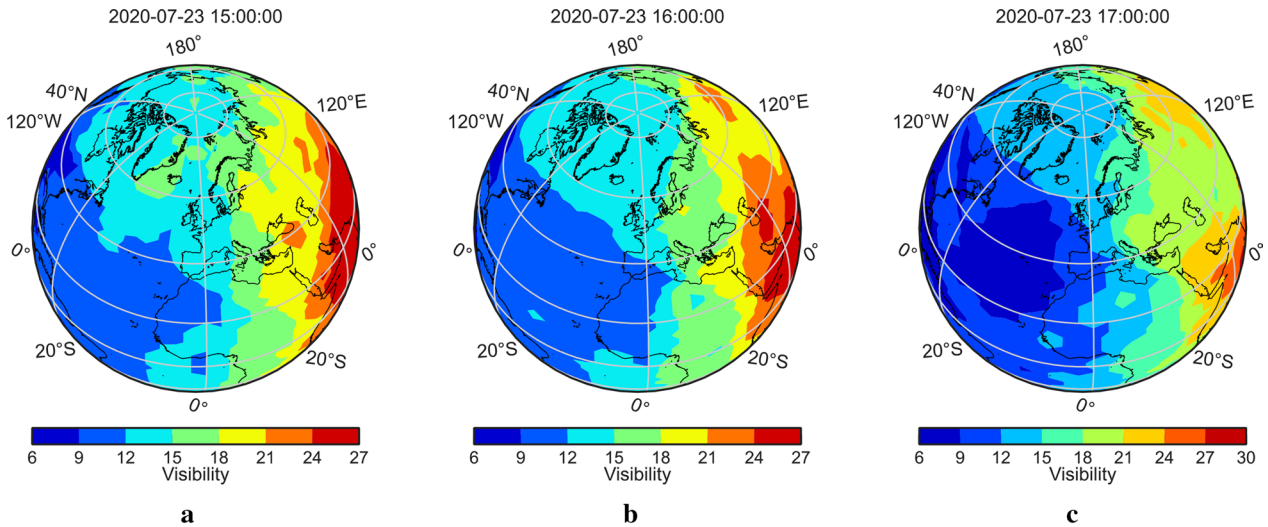

Fig. 2 The number of the visible BDS satellites with elevation angles above 5° at **a** GPS time 15:00:00, **b** 16:00:00, and **c** 17:00:00 on July 23, 2020. To highlight Britain and its surrounding areas, the far side of the globe is not displayed (the same below)

GLONASS at a sampling interval of one second with an Android app GEO++RINEX (Receiver INdependent EXchange format) Logger ver. 2.1.6 and the observed data were stored in the phone in RINEX 3.03 format. Figure 6 shows the locations of these two experiments.

The static observation point was in the middle of an open meadow in the park, where the smartphone was placed in its natural state and logged the GNSS data for two hours (14:47:42–16:47:41 UTC). The kinematic experiment was done in a complex observation scenario. As shown in Fig. 6b, the experimenter held the smartphone to collect the GNSS observations for about 18 min (14:15:01–14:33:03 UTC) along Wollaton Park Lake in the counterclockwise direction. The red line represents the approximate walking trajectory, and the yellow landmark represents the start and end points. The lakeside path is mostly covered by trees, which is a challenging environment for GNSS positioning. The experimenter passed through two dense forest areas, and the rest is semi-open spaces interlaced with fully sheltered environments. In the process of kinematic data collection, the vegetation canopy can block the satellite signals, resulting in signal attenuation or loss of lock, and cause complicated multipath effects. Furthermore, the huge lake is also a potential source of multipath interference.

Released in October 2018, the Huawei Mate 20 uses Kirin 980 chipset, which can receive satellite signals from BDS, GPS, GLONASS, Galileo and QZSS, and supports dual-frequency positioning (except BDS and GLONASS). Table 1 describes the general situation of the satellite signals received by the smartphone in our static experiment. A total of 12 BDS satellites, including 6 BDS-2 satellites and 6 BDS-3 satellites, were tracked, and their observations on B1I frequency were recorded in the data file.

The basic information on the received BDS satellites is listed in Table 2 (IGS MGEX 2020).

It should be noted that the Huawei Mate 20 cannot capture all the BDS satellite signals that are available due to the potential limitations of its chipset and antenna. As of the time of the manuscript revision, some newly released smartphones can track more BDS satellites than the Huawei Mate 20, such as Huawei Mate 40 Pro, which was launched in October 2020 with a Kirin 9000 chipset. This hardware defect will affect the performance of BDS mobile location services to a certain extent. Up to 15 GPS satellites were tracked in this test. L1 observations of these GPS satellites were recorded, of which 6 were also observed on L5 frequency. 7 Galileo satellites were tracked, but none of their observations on E1 frequency were recorded. The sky plots of the observed satellites for four GNSS constellations are shown in Fig. 7.

GPS has the best visibility and Galileo the worst. Note that C06, C09 and C16 are BDS IGSO satellites with poor observation conditions in the UK (C09 is slightly better). However, if certain conditions are met, such as elevation mask, they can also be considered for the mobile localization, for their inclusion can enhance the satellite distribution geometry.

There are pseudorange, carrier phase, Doppler and Carrier-to-Noise density ratio (C/N0) measurements on each available frequency in the data file. Due to the implementation of power duty cycling, continuous and stable smartphone carrier phase observations may not be obtained by the Huawei Mate 20. But this does not affect

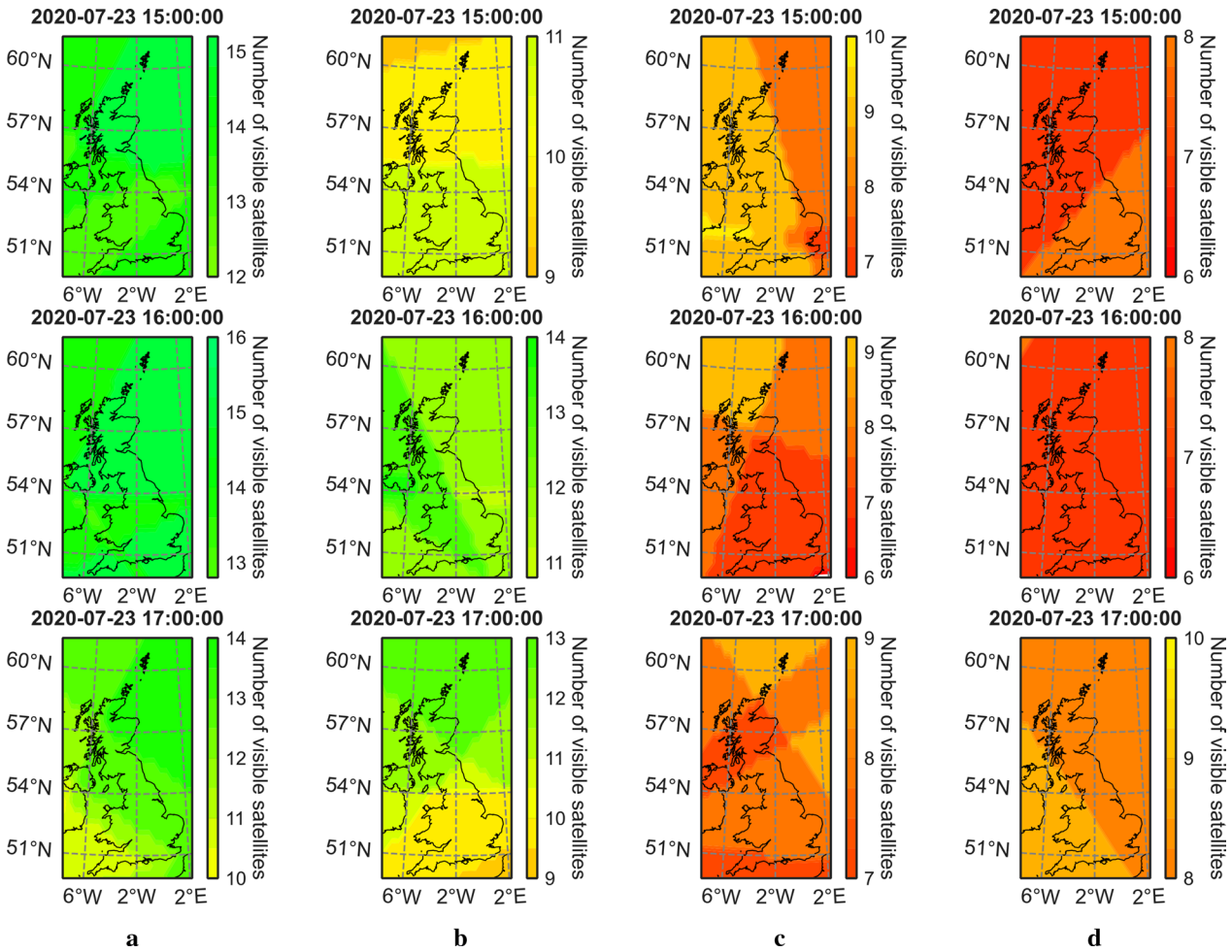

Fig. 3 The number of the visible satellites for **a** BDS, **b** GPS, **c** Galileo and **d** GLONASS at three moments in the UK territory

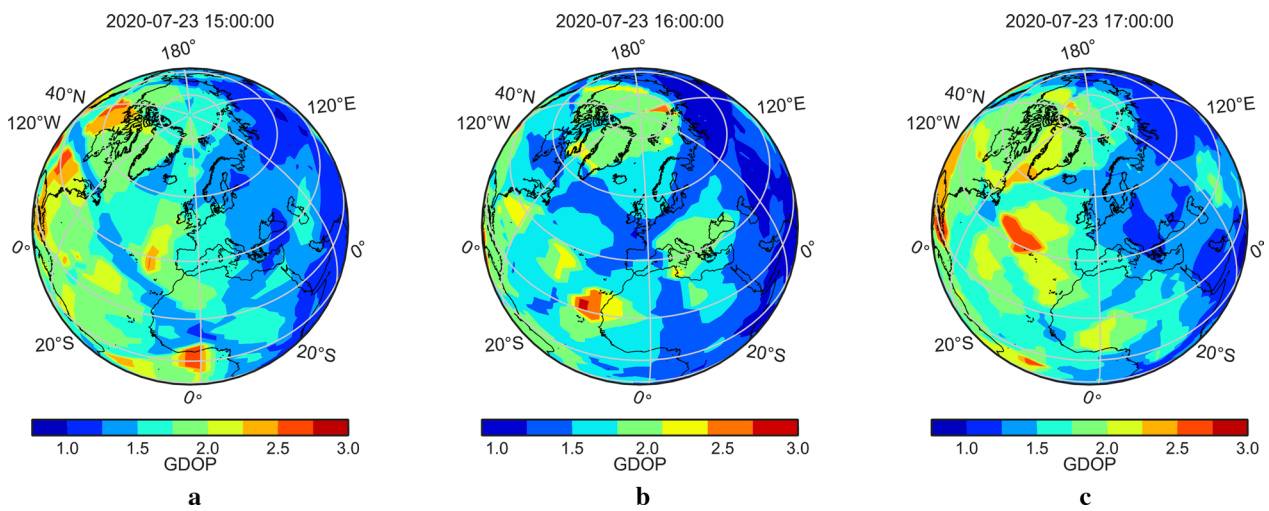

Fig. 4 GDOP distribution of BDS satellites with elevation angles above 5° at **a** GPS time 15:00:00, **b** 16:00:00, and **c** 17:00:00 on July 23, 2020

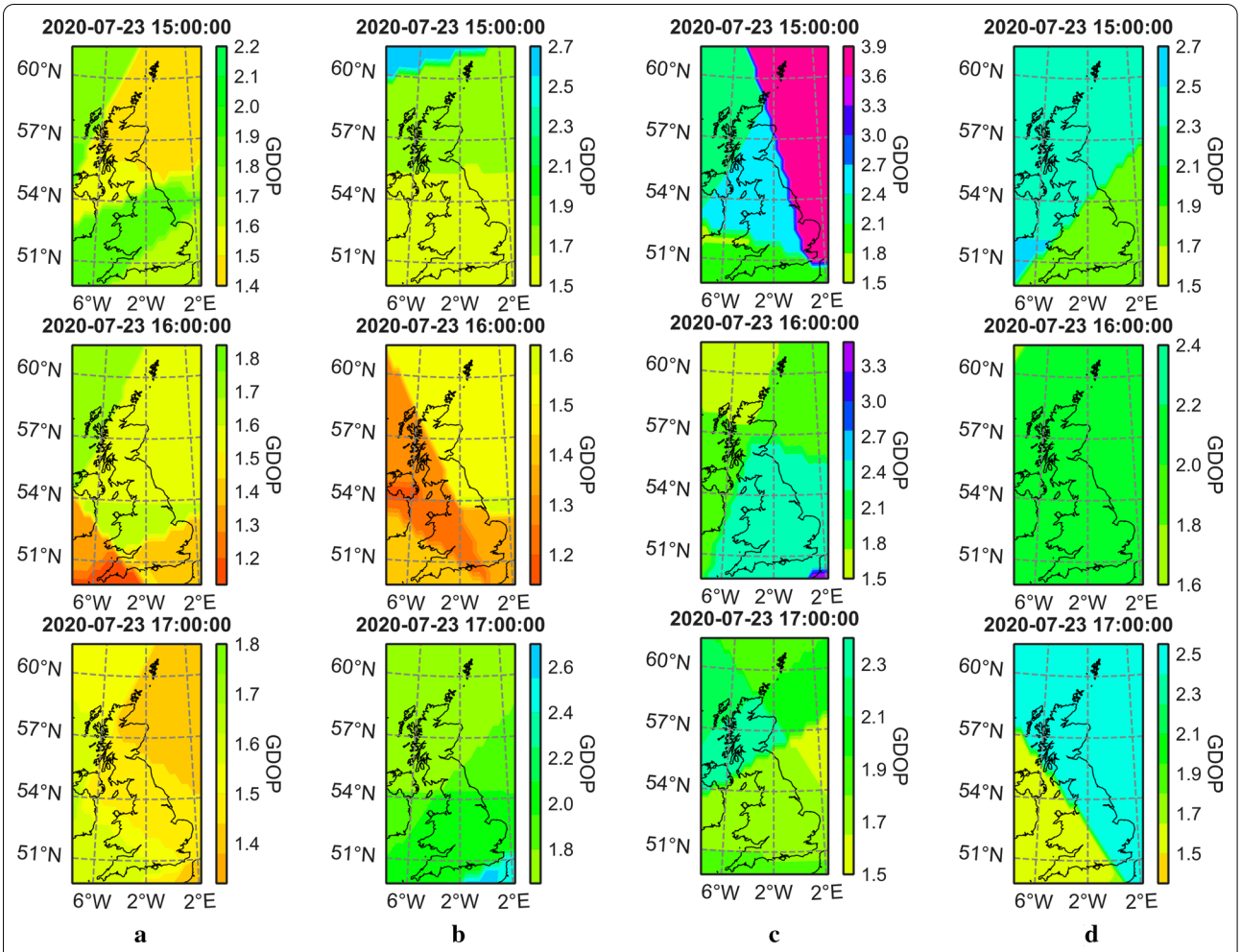

Fig. 5 GDOP distribution of satellites for **a** BDS, **b** GPS, **c** Galileo and **d** GLONASS at three moments in the UK territory

Fig. 6 Locations for **a** static and **b** kinematic smartphone GNSS data collection and their surrounding environments

Table 1 GNSS observations collected using Huawei Mate 20 and Geo + + RINEX Logger

Constellation	Frequencies	Notes
BDS	B1	6 BDS-2 satellites and 6 BDS-3 satellites were tracked
GPS	L1, L5	15 GPS satellites broadcast signals on L1 and 6 of them also broadcast on L5
Galileo	E1, E5a	E5a observations of 7 Galileo satellites and no E1 observations were recorded
GLONASS	G1	12 GLONASS satellites were tracked

Table 2 Details of BDS-2 and BDS-3 satellites received by the Huawei Mate 20

PRN	Common name	Int. Sat. ID	Orbit	Launch date
C06	BDS-2 IGSO-1	2010-036A	~117°E	2010-07-31
C09	BDS-2 IGSO-4	2011-038A	~95°E	2011-07-26
C11	BDS-2 MEO-3	2012-018A	between slots A-6 and A-7	2012-04-29
C12	BDS-2 MEO-4	2012-018B	between slots A-7 and A-8	2012-04-29
C14	BDS-2 MEO-6	2012-050B	between slots B-3 and B-4	2012-09-18
C16	BDS-2 IGSO-7	2018-057A	~112°E	2018-07-09
C21	BDS-3 MEO-3	2018-018B	Slot B-5	2018-02-12
C26	BDS-3 MEO-12	2018-067A	Slot C-2	2018-08-24
C27	BDS-3 MEO-7	2018-003A	Slot A-4	2018-01-11
C28	BDS-3 MEO-8	2018-003B	Slot A-5	2018-01-11
C33	BDS-3 MEO-14	2018-072B	Slot B-3	2018-09-19
C34	BDS-3 MEO-15	2018-078B	Slot A-7	2018-10-15

our data quality analysis and positioning performance evaluation. In addition to BDS, we also studied three other constellations for comparison.

Smartphone BDS observation quality assessment

In this section, we evaluate the quality of the BDS data based on the static observations in the open scenario. The evaluation includes signal carrier-to-noise density ratio and pseudorange noise. The comparative analyses with GPS, GLONASS and Galileo are also provided.

Carrier-to-noise density ratio

C/N0 is an important and a frequently used indicator to measure the signal quality of a satellite. It is a normalized expression of Signal-to-Noise Ratio (SNR) and determines the precision of the computed pseudorange and carrier phase (Sharawi et al. 2007). In general, a higher C/N0 value means the better quality of observations. The magnitude of C/N0 is not only affected by the satellite antenna and signal propagation path, but also closely related to the receiving hardware. The C/N0 measurements of a smartphone is about 10 dB·Hz lower than that of geodetic-grade equipment (Zhang et al. 2018; Paziewski et al. 2019).

Figure 8 depicts the variation trend of the average C/N0 of each satellite on BDS B1, GPS L1, Galileo E5a and GLONASS G1 frequencies relative to the elevation angle with a spacing of 1°. The C/N0 value usually has some positive correlation with the elevation angle of the satellite, but the C/N0 values of some satellites attenuate at high elevation angles, and even show large oscillations. Overall, the best performer in this regard is Galileo. From the subgraph of BDS, one can see that BDS-3 is apparently superior to BDS-2. The C/N0 of the former is more stable than that of the latter, and the C/N0 value of BDS-3 is also much greater than BDS-2 at medium–high elevation angles.

To make a clearer comparison of the C/N0 of BDS with that of the other three systems, we counted the C/N0 measurements of the satellites at elevation angles above 45° and calculated their mean and standard deviation. The results are shown in Fig. 9. In the figure, μ and σ represent the above two statistics, respectively.

The average C/N0 of BDS reaches 35.2 dB·Hz, which is lower than GPS but higher than Galileo and GLONASS. However, its standard deviation of 5.4 dB·Hz is the highest among the four systems. This is mainly due to the inconsistent C/N0 measurements between BDS-2 and BDS-3. Figure 10 shows the respective C/N0 statistics of the two subsystems. From the figure, the average C/N0 of BDS-3 is significantly greater than that of BDS-2, and the standard deviation is smaller, which indicates that BDS-3 has improved the quality on the retained signals as well.

Pseudorange measurement noise

For GNSS single-frequency single point positioning, the phase minus code combination is often used to verify the consistency between code and the phase observations. The combination contains ambiguity parameter, ionospheric delay, hardware delay, multipath error, and observation noise. The first two can be considered constants in a short term, and the latter three change with time. However, the duty cycling mode of a smartphone causes cycle slips at each epoch, and the phase observation is no longer stable (Riley et al. 2018). To

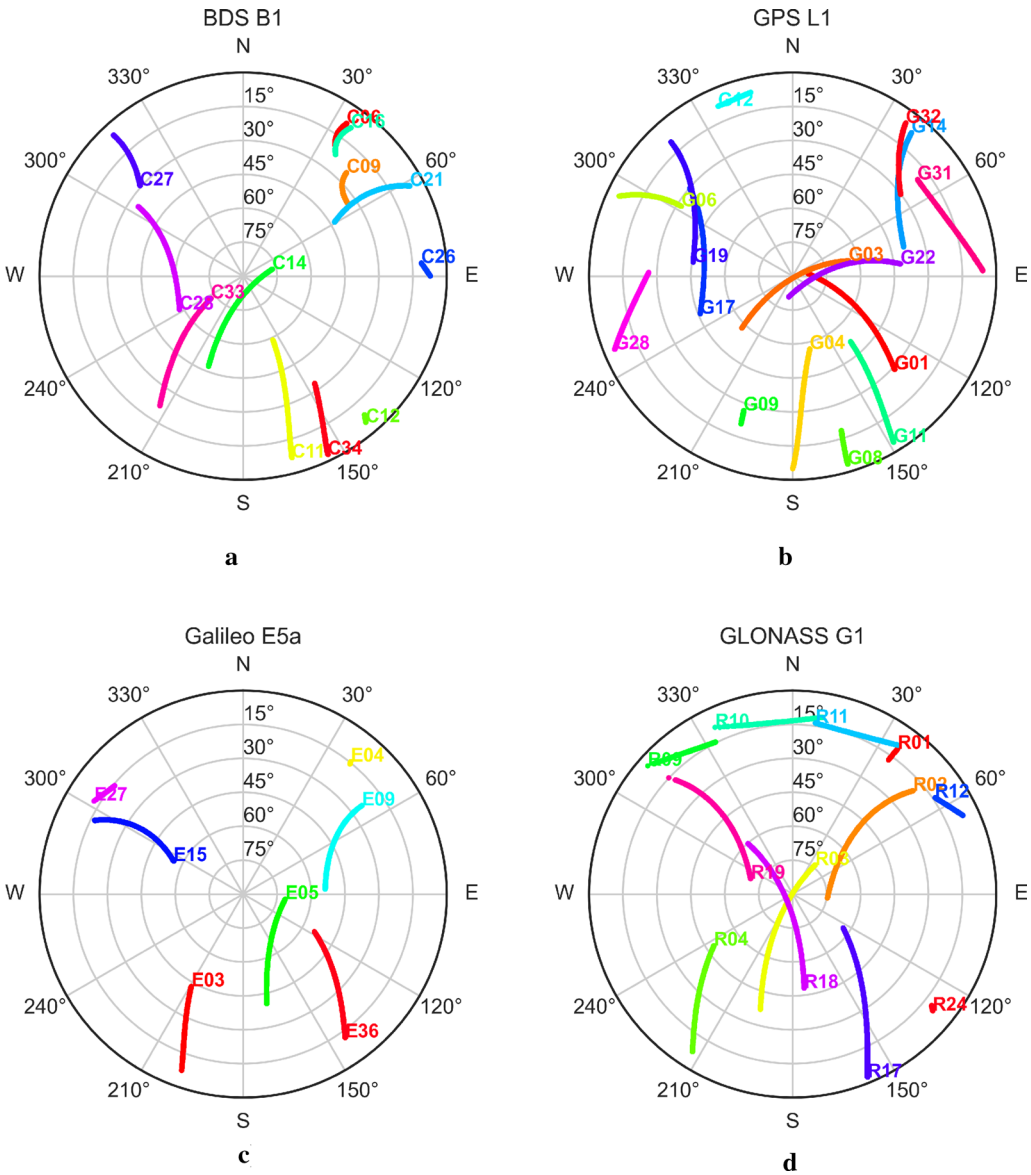

Fig. 7 Sky plots of the observed satellites on **a** BDS B1, **b** GPS L1, **c** Galileo E5a and **d** GLONASS G1 for two hours

obtain a stationary time series, the single differencing is made for the combination in the time domain. The Time-Differenced (TD) phase minus code combination (de Bakker et al. 2009) eliminates the ambiguity term and greatly reduces the influence of ionospheric delay, hardware bias and multipath effect. Therefore, the residuals reflect pseudorange noise, even though the noise is amplified by the differencing process. Here we normalized the standard deviation of the differenced combination to the undifferenced level.

Figure 11 shows the phase minus code combinations and their TD values on BDS B1, GPS L1, Galileo E5a and GLONASS G1 frequencies.

The satellites with longer observation time are selected for illustration. Note that the smartphone interrupted data recording at the 4230th second. We can see that due to the influence of duty cycling the phase minus code combinations of BDS, GPS and Galileo satellites all drift to different degrees, which indicates the increasing divergence between carrier phase and pseudorange observations within an observation episode until a large cycle

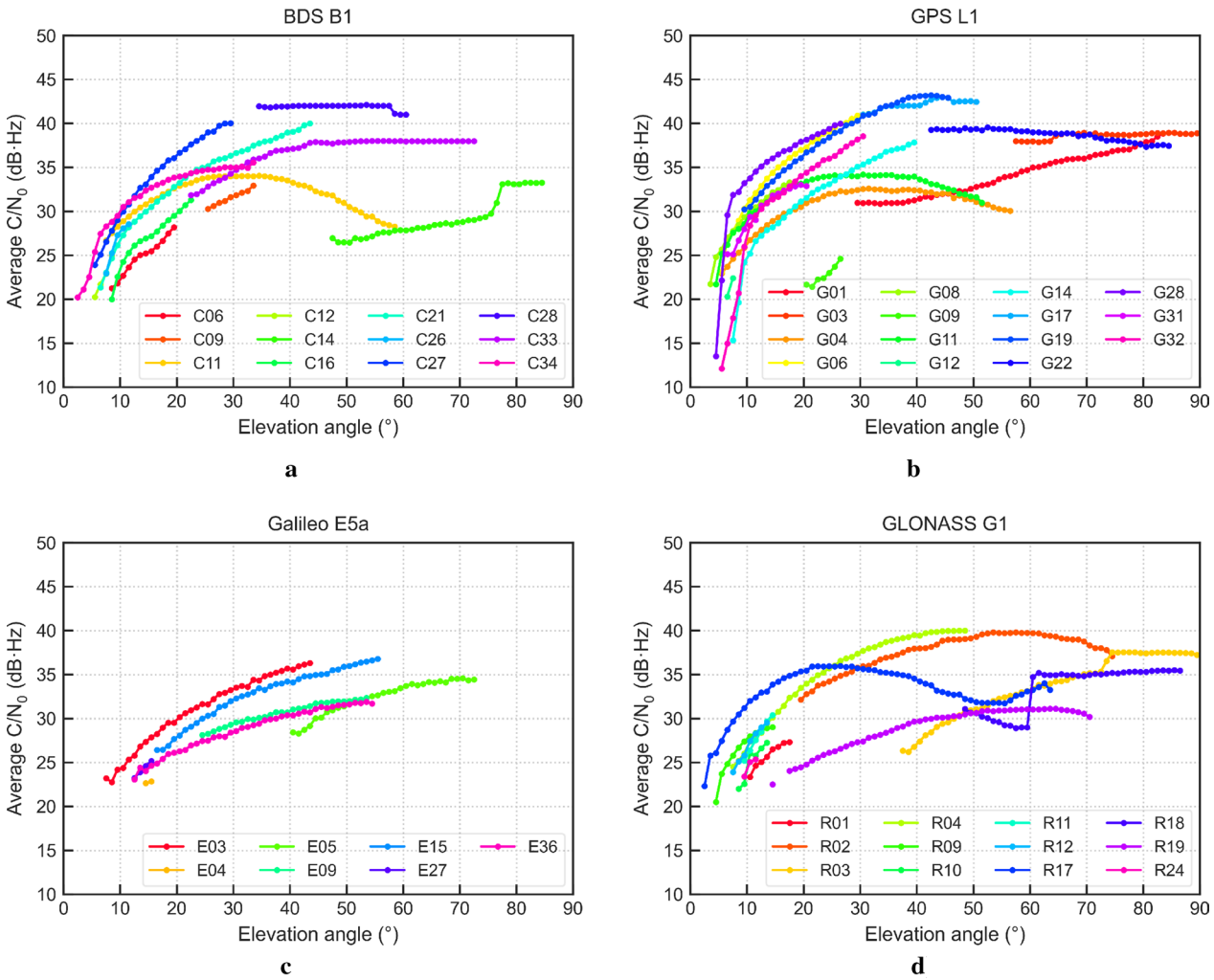

Fig. 8 Average C/N0 versus the elevation angles of the observed satellites on **a** BDS B1, **b** GPS L1, **c** Galileo E5a and **d** GLONASS G1 frequencies

slip occurs. According to Paziewski et al. (2019), this phenomenon is caused by the receiver clock-related effect, that is, inconsistency between the smartphone phase and the code clocks in the duty cycling mode. Compared with GPS and Galileo, BDS shows the fastest drift with a significant linear trend. There is no obvious regularity in the drift of Galileo phase-code combinations. However, the above drift does not occur for GLONASS satellites. The exact reason is not yet clear, but it is speculated that this may be related to the signal system (Frequency Division Multiple Access, FDMA) adopted by GLONASS that is different from the other three constellations.

Ignoring the occasional spikes caused by large cycle slips, the time series of the TD phase-code combinations shown in Fig. 11 are fluctuating around zero. Their amplitudes reflect the noise level of the pseudorange observations. We normalized the standard deviation of the TD phase-code combinations for 12 satellites, and the results are shown in Fig. 12.

The pseudorange noise of Galileo satellites is the smallest overall, and BDS is better than GPS, smaller than 0.5 m. Besides, BDS and Galileo satellites show better noise consistency among themselves. In contrast, the pseudorange noise of GLONASS satellites varies greatly, ranging from 0.05 m to 2.51 m. The different frequencies of different GLONASS satellites seem responsible for this significant discrepancy in the pseudorange measurement errors if no satellite fails. From the perspective of orbital types, C09, C11 and C28 are IGSO, MEO and MEO satellites, respectively, while C09 and C11 belong to BDS-2 and C28 to BDS-3. Nevertheless, their pseudorange noise levels at the same frequency are quite consistent.

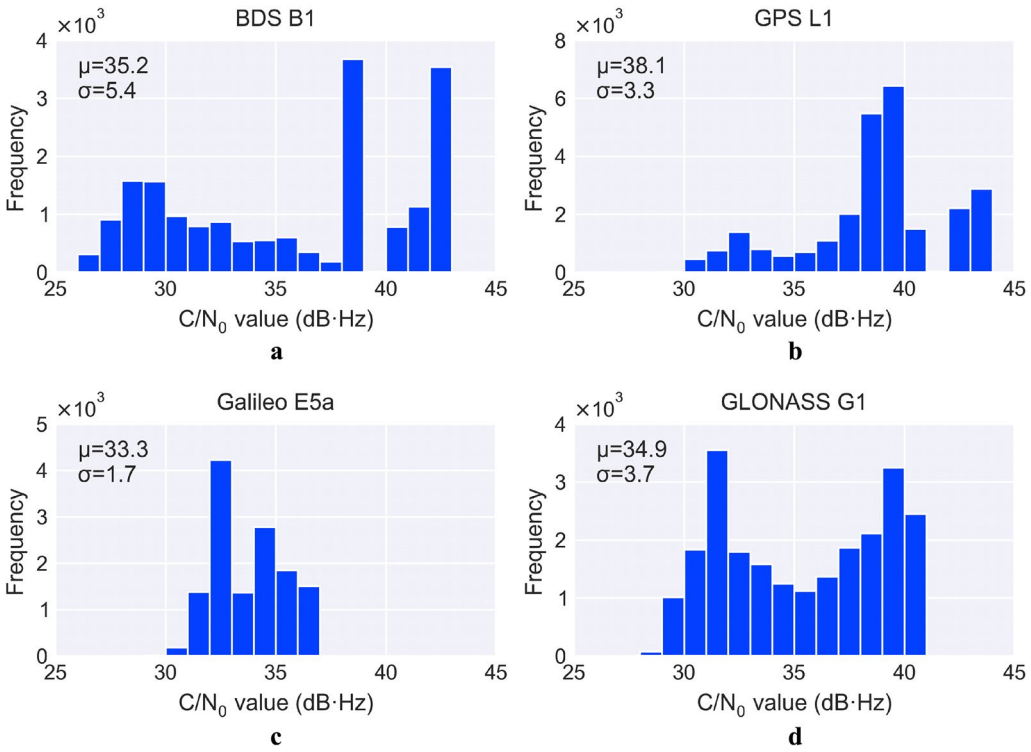

Fig. 9 Histogram and statistics of the C/N0 measurements of **a** BDS, **b** GPS, **c** Galileo and **d** GLONASS satellites at elevation angles above 45°

Figure 13 shows the time series of the C/N0 and elevation angles for these 12 satellites in the static experiment.

Only the pseudorange noise of Galileo and its satellite elevation or the C/N0 measurement show some correspondence, while the behavior of BDS, GPS and GLONASS is not obvious. Especially the noise mutation of G1, G19 and R02 around the 3000th, 1400th and 6000th second, respectively, fails to obtain a good response of elevation angle or C/N0. An interesting finding, however, is that the signal reception strength of GPS and Galileo satellites generally maintains a good positive correlation with the elevation angle, while the strength for BDS and GLONASS satellites does not. This suggests that BDS and GLONASS satellite signals are more susceptible to interference.

Evaluation of smartphone BDS positioning performance

In this section, we evaluate the smartphone BDS positioning performance based on the collected static and kinematic pseudorange observations on BDS B1, GPS L1, Galileo E5a and GLONASS G1 frequencies. At the same time, the positioning results of other systems are used for contrastive analysis, including single-system and multi-system positioning. In this study, the observation equations for undifferenced pseudorange P can be expressed as follows:

$$P_1^{\mathrm{C}} = \rho_{\mathrm{r}}^{\mathrm{C}} + t_{\mathrm{r}}^{\mathrm{C}} - t_3^{\mathrm{C}} + T_{\mathrm{r}}^{\mathrm{C}} + I_{\mathrm{r},1}^{\mathrm{C}} + \mathrm{DCB}_{B1-B3} + \varepsilon_{\mathrm{r},1}^{\mathrm{C}} \tag{1}$$

$$P_1^{\mathrm{G}} = C_1^{\mathrm{G}} + \mathrm{DCB}_{P1-C1} = \rho_{\mathrm{r}}^{\mathrm{G}} + t_{\mathrm{r}}^{\mathrm{G}} - t_{1,2}^{\mathrm{G}} + T_{\mathrm{r}}^{\mathrm{G}} + I_{\mathrm{r},1}^{\mathrm{G}} - \frac{1}{\gamma_2^{\mathrm{G}} - 1}\mathrm{DCB}_{P1-P2}^{\mathrm{G}} + \varepsilon_{\mathrm{r},1}^{\mathrm{G}} \tag{2}$$

$$P_5^{\mathrm{E}} = \rho_{\mathrm{r}}^{\mathrm{E}} + t_{\mathrm{r}}^{\mathrm{E}} - t_{1,5}^{\mathrm{E}} + T_{\mathrm{r}}^{\mathrm{E}} + \gamma_5^{\mathrm{E}} I_{\mathrm{r},1}^{\mathrm{E}} - \frac{\gamma_5^{\mathrm{E}}}{\gamma_5^{\mathrm{E}} - 1}\mathrm{DCB}_{E1-E5a} + \varepsilon_{\mathrm{r},5}^{\mathrm{E}} \tag{3}$$

$$P_1^{\mathrm{R}} = \rho_{\mathrm{r}}^{\mathrm{R}} + t_{\mathrm{r}}^{\mathrm{R}} - t_{1,2}^{\mathrm{R}} + T_{\mathrm{r}}^{\mathrm{R}} + I_{\mathrm{r},1}^{\mathrm{R}} - \frac{1}{\gamma_2^{\mathrm{R}} - 1}\mathrm{DCB}_{P1-P2}^{\mathrm{R}} + \varepsilon_{\mathrm{r},1}^{R} \tag{4}$$

where superscripts C, G, E and R denote BDS, GPS, Galileo and GLONASS satellite system, respectively; I and T are the ionospheric delay and tropospheric delay, obtained with the Klobuchar model and Saastamoinen model, respectively; DCB is the difference code bias, and its subscript clarifies the difference between the hardware delays in the measured pseudoranges; let S be the satellite system and j be the frequency, $t_{\mathrm{r}}^{\mathrm{S}}$ is the receiver clock bias that absorbs the code delay of the receiver; t_j^{S} is the

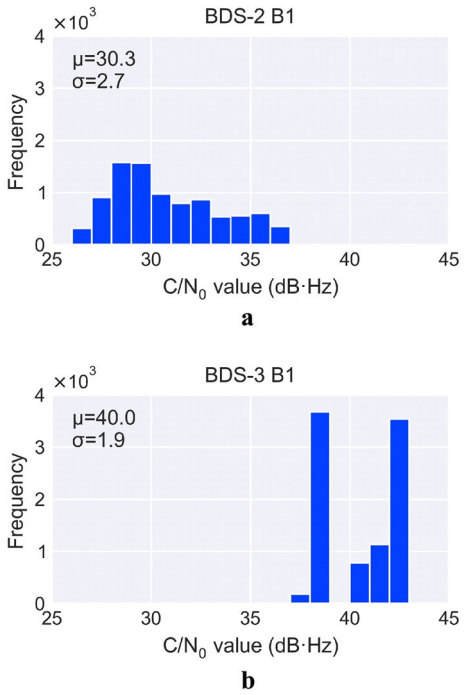

Fig. 10 Histogram and statistics of the C/N0 measurements of **a** BDS-2 and **b** BDS-3 satellites at elevation angles above 45°

satellite clock bias calculated using the broadcast ephemeris; $\gamma_j^S = \left(f_1^S/f_j^S\right)^2$ is the frequency-dependent scale factor.

The SPP solutions were obtained by adopting the weighted least squares (WLS) method based on satellite elevation angle, and the stochastic model is as follows (Takasu and Yasuda 2009):

$$\boldsymbol{W} = \mathrm{diag}\left(\sigma_1^{-2}, \sigma_2^{-2}, \ldots, \sigma_n^{-2}\right) \tag{5}$$

$$\sigma^2 = F^S\left(a_\sigma^2 + b_\sigma^2/\sin^2\theta\right) + \sigma_{\mathrm{eph}}^2 + \sigma_{\mathrm{ion}}^2 + \sigma_{\mathrm{trop}}^2 + \sigma_{\mathrm{bias}}^2 \tag{6}$$

where F^S is the satellite system error factor (1: BDS, GPS and Galileo, 1.5: GLONASS); a_σ and b_σ are code error factors; θ is the satellite elevation angle; σ_{eph}^2 is the variance of ephemeris and clock error; σ_{ion}^2 is the variance of ionosphere correction model error; σ_{trop}^2 is the variance of troposphere correction model error; σ_{bias}^2 is the variance of code bias error. For the reliable position solutions the Chi-square test was employed to verify the results. When the test fails, the position solution at that epoch is discarded. The elevation cutoff angle of the satellite was all set to 10°.

Static positioning analysis

Figure 14 illustrates the number of tracked satellites and GDOP values for each constellation during the two-hour static observation period.

At the epoch of the 4230th second in the top panel the number of the tracked satellites is zero. This indicates that the smartphone loses lock of all satellites. From the figure, GPS satellites have the best visibility at the static site with an average of about 10.0 visible satellites. BDS is in the second with an average number of 8.2. Before the 5455th second, the number of visible satellites remains about 8–9, but declines afterwards as some satellites drop below the elevation cutoff angle. Galileo has the smallest number of visible satellites with an average of 4.8, although the number is relatively stable for most of the time. Their GDOP values give a consistent interpretation. The ascending order of the overall GDOP value is GPS, GLONASS, BDS and Galileo, and their average GDOP are 1.8, 2.5, 2.7 and 9.7, respectively. The GDOP value of BDS increases significantly between the 6745th second and the 6935th second due to a decrease in the number of valid satellites, which raises its overall GDOP value. Galileo has very large GDOP values at the beginning and does not return to a relatively ideal geometry state until the 2031st second, but its GDOP is still the largest among the four systems for the rest of the time.

Figure 15 shows the relative horizontal locations obtained using the pseudorange observations of different systems and their combination.

The average value of GLONASS positioning results is selected as the origin of the topocentric coordinate system. Although there is no ground-truth value, we can evaluate the positioning performance by analyzing the dispersion of each set of positioning results. It is clearly seen that GLONASS has the worst positioning results due to its inconsistent ranging precision and inter-frequency code bias (Reußner and Wanninger 2012). In contrast, there are much better concentrations of BDS, GPS and Galileo positioning results. The positioning precision of BDS and GPS in the east direction is better than that in the north direction, while Galileo position solutions are very close together in the north direction but scattered in the east direction. Since the positioning results of GLONASS are not satisfactory, it is not included in the multi-system SPP solutions. The figure shows that the fusion of BDS B1, GPS L1 and Galileo E5a code observations significantly improve the positioning precision, which is thanks to the increase in the number of valid satellites and the enhancement of geometric distribution of satellites. The concentration of the position solutions is high and there are no obvious outlying points. The increased availability of positioning results from a multi-constellation system

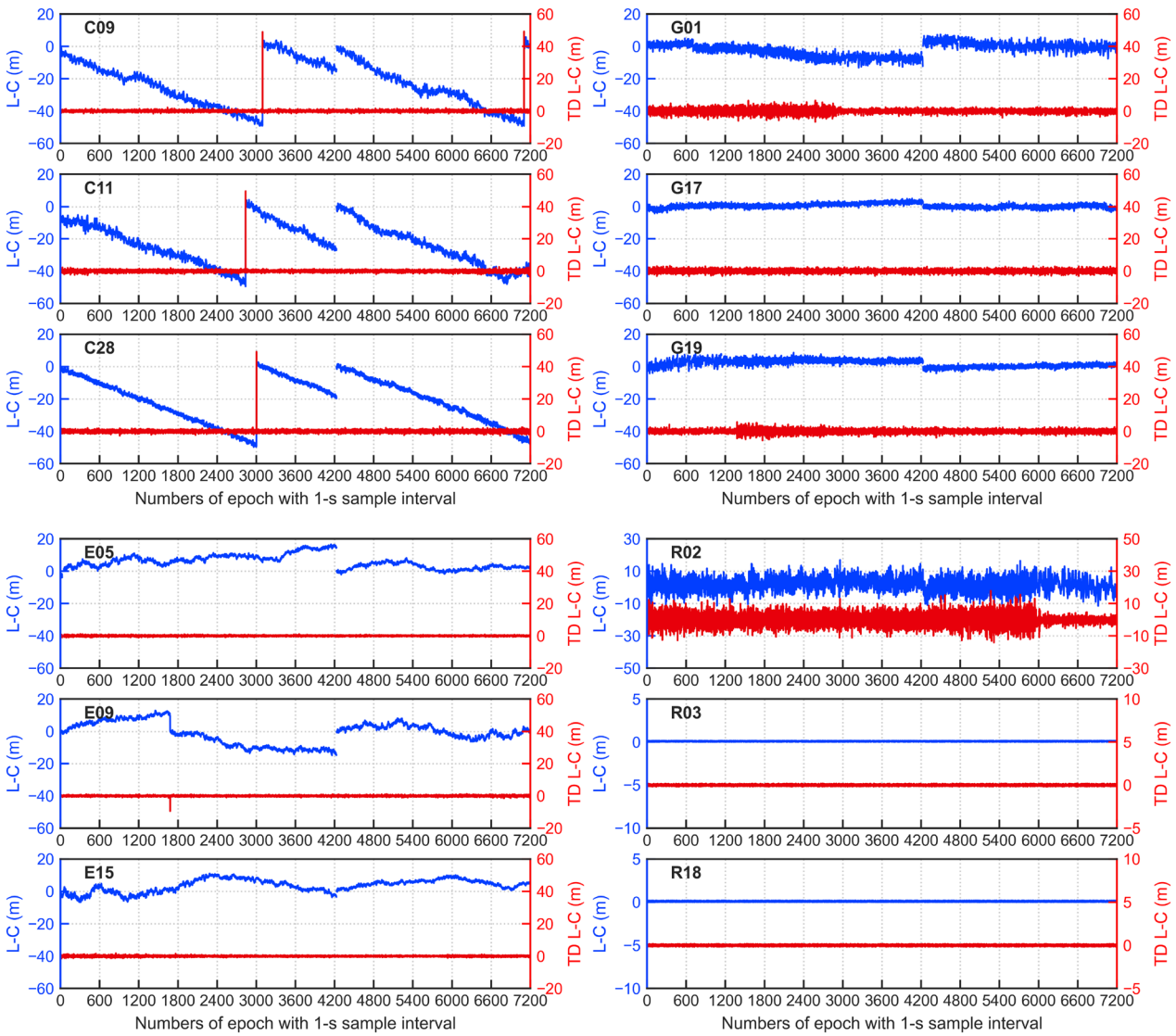

Fig. 11 Phase minus code combinations (blue) and time-differenced values (red) of BDS, GPS, Galileo and GLONASS satellites

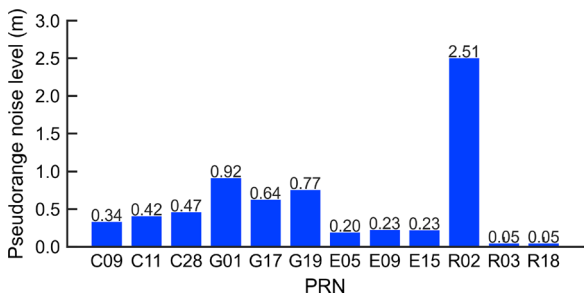

Fig. 12 Pseudorange noise levels of 12 BDS, GPS, Galileo and GLONASS satellites

is another apparent benefits. Some position solutions were excluded due to the failure of the Chi-square test. In the static smartphone positioning, BDS and the BDS/GPS/Galileo combination output the positioning results for all 7199 valid epochs, while for GPS, Galileo and GLONASS the position solutions of 1, 117 and 31 epochs, respectively, were discarded. In addition, Galileo has no position outputs for 20 epochs because the number of observed satellites is below 4. It can be seen that the quality of BDS position solutions is quite high, and multi-system fusion can significantly improve the availability of positioning results.

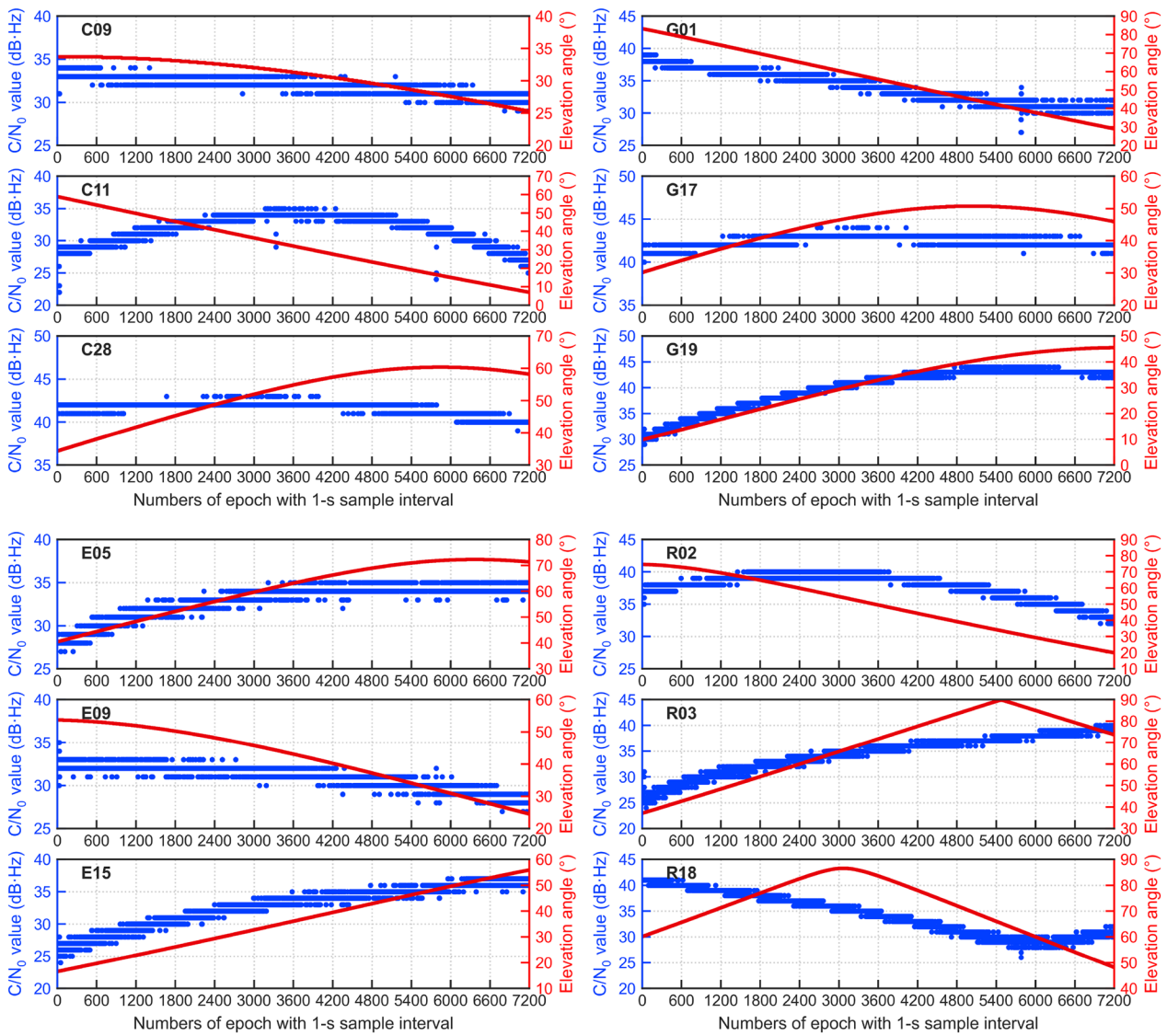

Fig. 13 C/N0 (blue) and elevation angle series (red) of BDS, GPS, Galileo and GLONASS satellites

In order to further quantify the above positioning results, we calculated their horizontal position deviations at each epoch by using the following formula:

$$\delta_H = \sqrt{\delta_E{}^2 + \delta_N{}^2} \tag{7}$$

where δ_E and δ_N are the position deviations in the east and north directions, respectively. The position deviation used here refers to the difference between a determined position and the reference position, which is the mean of the positioning results with the corresponding satellite system. Figure 16 illustrates the probability distribution of the smartphone horizontal positioning deviation using the pseudorange observations from different satellite systems.

The Circular Error Probable (CEP) is one of the important measures for the position accuracy of a navigation system, and for the air and land applications the most used statistical measure is 95% Radius (R95) value (Specht et al. 2019), which is defined as the radius of the circle centered at the reference position, containing the position estimate with probability of 95%. The R68 (2D) and R95 (2D) values are list in Table 3.

As expected, the BDS/GPS/Galileo, has the smallest R95 value of horizontal position solutions, followed by Galileo. Although Galileo position solutions in the east direction are relatively scattered, its positioning results in the north direction are more concentrated, so that its horizontal positioning performance is the best in

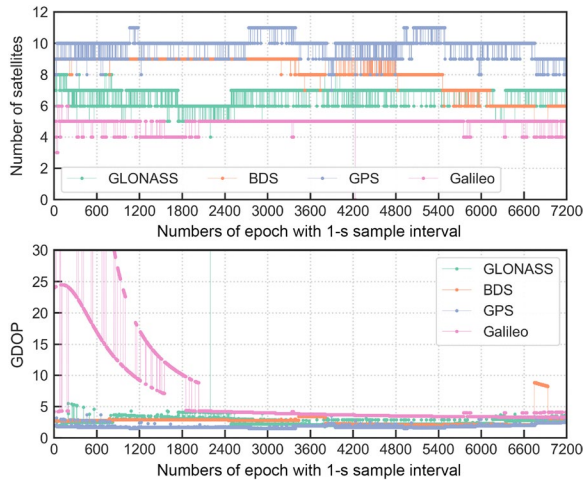

Fig. 14 Numbers of visible satellites and GDOP values of four systems in the static test

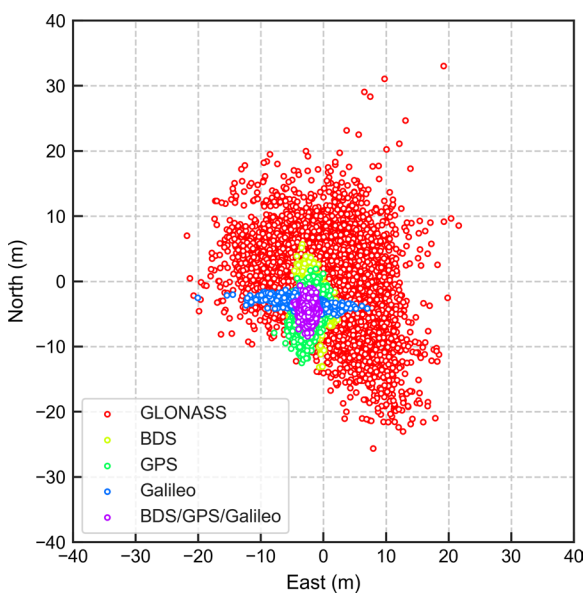

Fig. 15 Static smartphone positioning results based on different satellite systems and their combination

the single-system positioning. On the other hand, the high pseudorange precision of Galileo support the good smartphone SPP performance. For BDS, its horizontal R95 value reaches 2.88 m, which is greater than Galileo, but less than GPS and GLONASS. And a similar situation occurs for the R68 (2D), which is 1.43 m for BDS. Notably, the R68 value of Galileo is only 0.67 m, smaller than that of BDS/GPS/Galileo, which is 0.90 m. Despite this, the deviations of Galileo are in the range of 0.67 m to 2.17 m, which still account for a considerable proportion, lowing its overall horizontal precision.

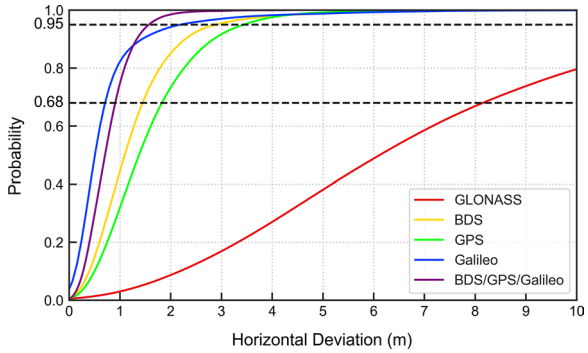

Fig. 16 Cumulative probability of smartphone horizontal position deviation based on different satellite systems

Table 3 2D positioning deviations of Huawei Mate 20 based on different satellite systems

Probability	2D positioning deviations based on different satellite systems (m)				
	BDS	GPS	Galileo	GLONASS	BDS/GPS/Galileo
68%	1.43	1.81	0.67	8.10	0.90
95%	2.88	3.44	2.17	15.23	1.56

Figure 17 displays the positioning deviations in the three directions in the time domain based on different systems.

Before the 2000th second, Galileo positioning deviations in the east and up directions are relatively large, only smaller than GLONASS. Compared with Fig. 14, we can find that this is due to the very large GDOP values of Galileo during this period. Similarly, the poor satellite geometry between the 6745th second and the 6935th second leads to relatively large deviations in BDS positioning results in the north direction. From Fig. 17, one can see the positioning results of the BDS/GPS/Galileo fusion are concentrated and stable in the three directions, which indicates the multiple systems can improve positioning performance. Regarding the single-system positioning, BDS shows the satisfactory performance of smartphone positioning in all three directions, as well as GPS. The positioning deviation of Galileo after the 2000th second is small, comparable to the BDS/GPS/Galileo.

Since the positioning deviation is a time series with zero mean, we can calculate the standard deviation to measure the positioning precision. The results are listed in Table 4.

The maximum deviation is also given to assess the stability of the positioning results. As can be seen, the horizontal positioning precision of BDS is superior to GPS and GLONASS, and its vertical precision is better than

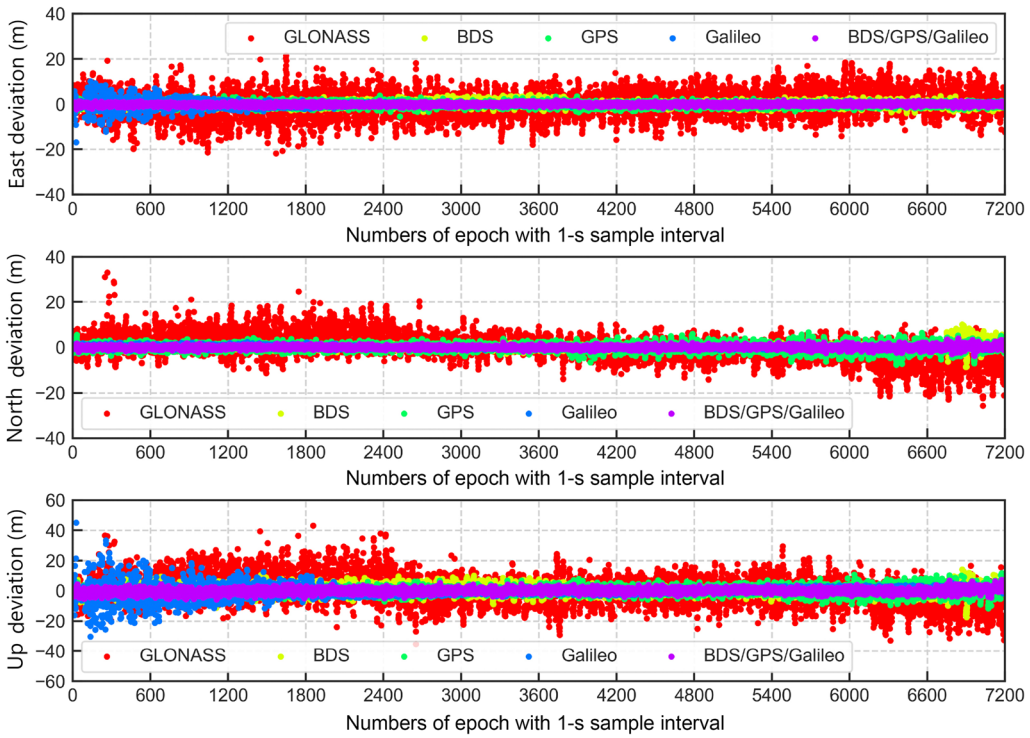

Fig. 17 Smartphone positioning deviation series in the east, north and up directions based on different systems

Table 4 Statistical results of smartphone positioning deviation

Constellation	Standard deviation in different directions (m)			Maximum absolute deviation in different directions (m)		
	East	North	Up	East	North	Up
BDS	1.09	1.16	3.02	4.30	10.09	17.37
GPS	0.97	1.57	2.45	5.43	7.79	11.71
Galileo	1.10	0.47	3.54	16.92	2.31	45.20
GLONASS	5.71	5.80	9.31	21.83	33.06	43.20
BDS/GPS/Galileo	0.54	0.70	1.51	2.31	3.90	7.27

Galileo and GLONASS. The standard deviations of BDS positioning results in the east, north and up directions are 1.09, 1.16 and 3.02 m respectively. Although Galileo positioning results are outstanding in the north direction, they do not achieve the same level of precision in the other two directions, and the maximum absolute deviations reach 16.92 and 45.20 m, respectively. The BDS/GPS/Galileo has the best performance both in positioning precision and stability. Despite more valid satellite and better geometric distribution, the horizontal precision of GPS is poorer than BDS. This is because of the smaller pseudorange noise of BDS.

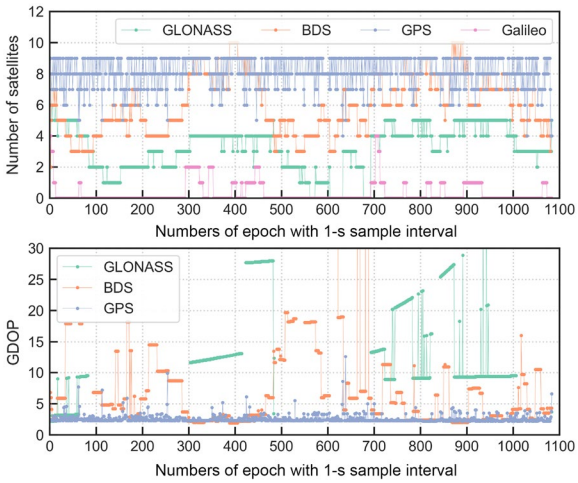

Fig. 18 Numbers of visible satellites and GDOP values of different systems in the kinematic experiment

Kinematic positioning analysis

In the kinematic positioning experiment, due to the complex observation environment the satellite signals were interfered and the number of visible satellites was also decreased. Figure 18 illustrates the situation where the satellite is blocked and the number of visible satellites for

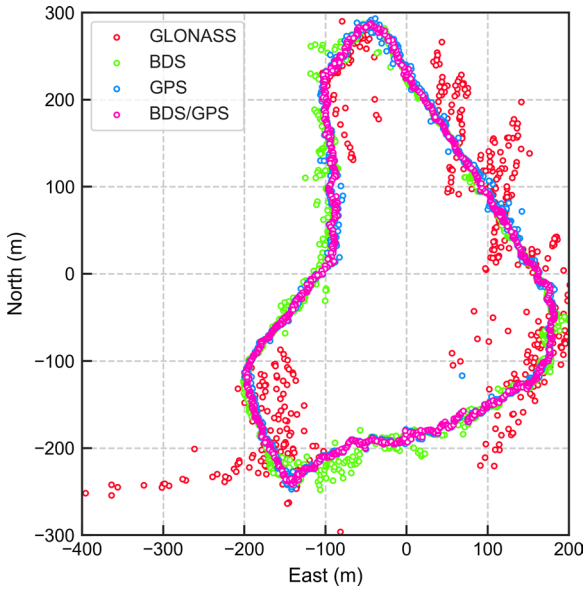

Fig. 19 Kinematic smartphone positioning results based on different satellite systems

each system was reduced compared with that in the static experiment.

The GPS satellites tracked by the smartphone were still the most, followed by BDS, GLONASS and Galileo. Their average number of observed satellites is 8.2, 6.1, 3.2 and 0.3, respectively. However, the number of the visible GPS satellites is more stable. In contrast, the numbers of the visible BDS and GLONASS satellites vary greatly. Galileo has only 8 epochs when 4 satellites are observed, and only 1 or 0 satellite visible in most of the observation period. From the variation trend of the numbers of the visible BDS and GLONASS satellites, the troughs of their broken lines correspond to the dense forest areas, indicating that this harsh environment has the least impact on GPS signals. Their GDOP values also confirm this. The GDOP values of GPS are small and stable with an average of 2.6, while those of BDS and GLONASS are very unstable, and GLONASS is the worst.

We performed smartphone positioning solutions for each satellite system, and the results are shown in Fig. 19.

The average value of GLONASS positioning results is selected as the origin of the topocentric coordinate system. Galileo is ignored because its visible satellites are too few. Obviously, the positioning results of the BDS/GPS fusion are the smoothest and well follow the motion trajectory. GPS performs best among the three systems, matching the track obtained with the BDS/GPS fusion. BDS is a bit inferior to GPS, especially in the dense forest areas. GLONASS has the worst performance, almost impossible to position in the dense forests.

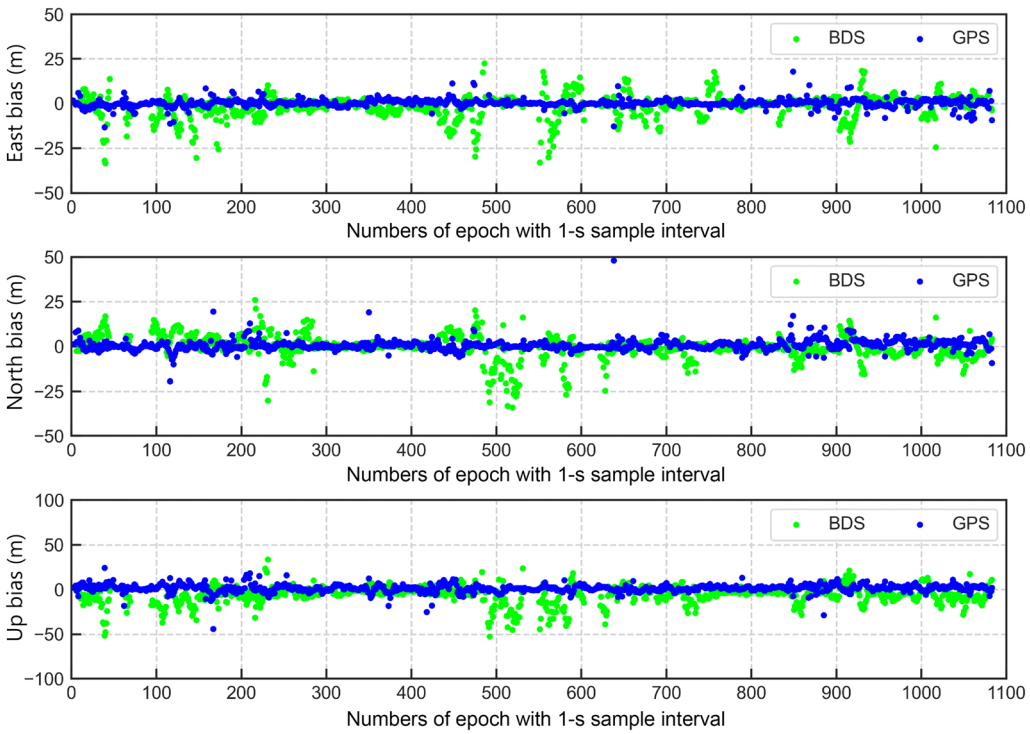

Fig. 20 Kinematic smartphone positioning biases of BDS and GPS with respect to the BDS/GPS combination

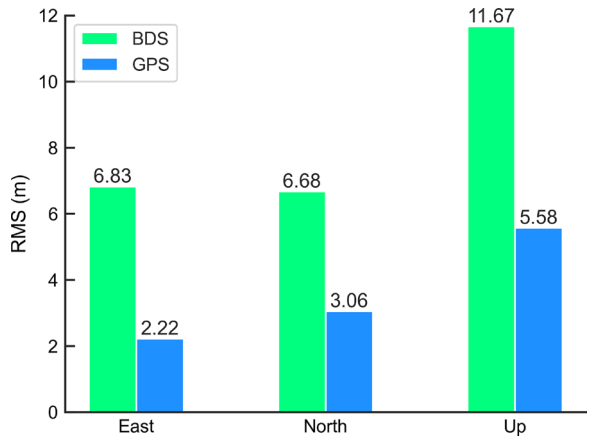

Fig. 21 Kinematic smartphone positioning bias RMS of BDS and GPS with respect to the BDS/GPS combination

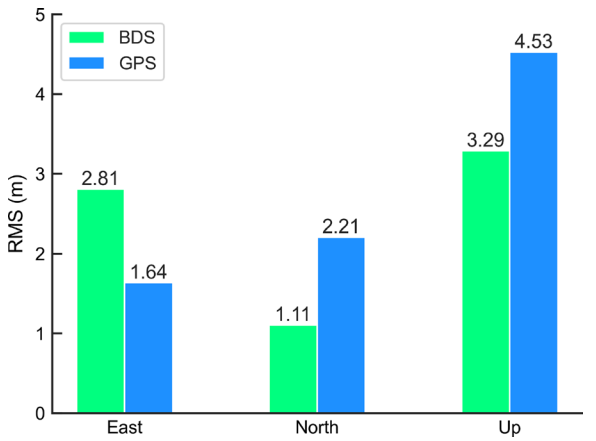

Fig. 23 Kinematic smartphone positioning bias RMS of BDS and GPS in the semi-open area

Figure 20 shows the positioning bias series of BDS and GPS in the three directions relative to the BDS/GPS fusion results.

The term bias used here refers to the difference between the determined position using a single satellite system and the position using the integrated BDS/GPS system. We can clearly see that the bias amplitude of GPS is smaller than that of BDS. Even in harsh environments, GPS positioning results can still maintain relatively good precision. On the contrary, the positioning performance of BDS is greatly affected by the environment, which is illustrated by the results at about the 0–280th second and the 440th–750th second. The bias Root Mean Squares (RMS) of BDS and GPS in the east, north and up directions are shown in Fig. 21. Only from the perspective of experimental results, the smartphone kinematic positioning performance of BDS in complex environments is not comparable to GPS. However, it cannot be ruled out that the degradation of smartphone BDS positioning performance is limited by the hardware of the phone.

We also selected a typical semi-open area for the positioning comparison of BDS and GPS. Figure 22 shows the data collection path and its surrounding environment, and the corresponding epochs were between the 290th second and the 430th second.

Similarly, we calculated their respective positioning bias RMS relative to the BDS/GPS fusion results. From

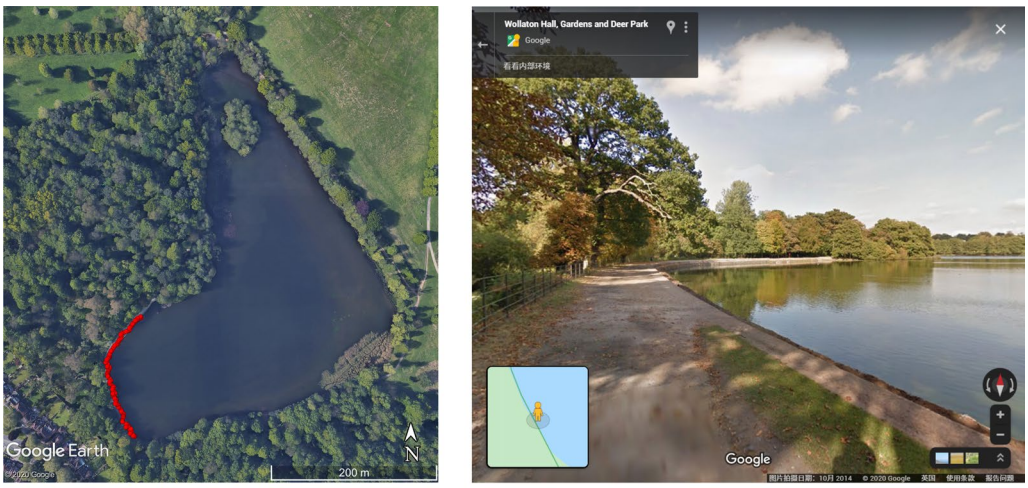

a **b**

Fig. 22 **a** A semi-open area and **b** its actual view in the kinematic scenario

Fig. 23, although the bias RMS of BDS in the east direction is greater than GPS, it is smaller in the north and up directions. This indicates that once the observation environment gets better, the kinematic positioning performance of BDS will improve significantly, even surpassing GPS.

Conclusions

To fully evaluate the performance of BDS positioning outside Asia–Pacific regions for mobile location-based services, the static and kinematic GNSS data in Nottingham, UK were collected with Huawei Mate 20 smartphone. The tests were conducted in an open meadow for static mode and lakeside wooded area for kinematic mode. We estimated the signal carrier-to-noise density ratio, pseudorange measurement noise, and positioning performance of BDS satellites in detail, and compared the results with GPS, Galileo and GLONASS. Some major findings are summarized as follows:

1. BDS can provide location services with good satellite visibility. BDS has the largest number of nominally visible satellites in the UK compared to any other system. Its signal carrier-to-noise density ratio is comparable to GPS. The signal quality of BDS-3 is generally better than BDS-2 on B1 frequency. Moreover, the selected BDS satellites have low pseudorange noise within 0.5 m, which is larger than Galileo satellites at 0.23 m level.
2. The horizontal precision of BDS positioning in an open environment is better than GPS with the R95 value of 2.88 m, even though its satellite geometry is poorer than GPS. The high precision using Galileo is limited by the number of visible satellites, and the positioning results cannot be consistent in the time domain. GLONASS has the worst positioning results due to its discrepant ranging precision and inter-frequency code bias. The inclusion of BDS into multi-system can significantly improve the positioning performance.
3. In the complex environment, the kinematic positioning performance of each satellite system degrades due to signal occlusion and reflection, but the results of GPS are least affected by environmental factors. Galileo satellites can rarely be tracked, and the GLONASS positioning results deteriorate the most. Despite the degradation, the BDS positioning results are usable for LBS users. In the semi-open area, the positioning performance of BDS quickly recovers to compete with GPS.

In summary, BDS alone can fully meet the requirements of global location services, especially in open environments, because of its good satellite visibility and ranging precision. However, in a harsh environment, the number of BDS satellites tracked by the smartphone is susceptible to environmental factors. It is worth noting that due to the limitation of smartphone GNSS chipsets, most of the current smartphones cannot receive the new BDS-3 signals with higher strength, or even track all the existing BDS satellites, which restricts the observation availability and positioning accuracy of BDS. The advancement of smartphone hardware in the future will inevitably enhance the positioning performance of BDS to a new level. Finally, the positioning of BDS integrated with other navigation satellite systems can greatly improve the accuracy and reliability of position solutions.

Acknowledgements

We gratefully acknowledge MGEX and GFZ for providing multi-GNSS orbit products and Dr. Pan Li for sharing the drawing method of global satellite visibility on his public platform. Thank Professor Yongqi Chen and the editor for their careful proofreading which has improved the quality of this manuscript. The first author is grateful for the sponsorship of the China Scholarship Council.

Authors' contributions

Conceptualization, X.M.; methodology, Y.X.; formal analysis, Y.X. and Q.Z.; data curation, Y.X.; writing-original draft preparation, Y.X.; writing-review and editing, Y.Y. and W.G.; supervision, S.P. and X.M. All authors read and approved the final manuscript.

Funding

This research was funded by the National Natural Science Foundation of China (41774027), the National Key Research and Development Program (2016YFB0502101), the Postgraduate Research & Practice Innovation Program of Jiangsu Province (KYCX19_0067) and the CoDRIVE demonstration project funded under the European Space Agency's Business Applications initiatives (ESA CoDRIVE Contract Number: 4000126688/19/NL/FGL).

Availability of data and materials

The smartphone GNSS observations used and analyzed in this study were collected by the first author.

Competing interests

The authors declare that they have no conflict of interest.

Author details

[1] School of Instrument Science and Engineering, Southeast University, Nanjing 210096, China. [2] Key Laboratory of Micro-Inertial Instrument and Advanced Navigation Technology, Ministry of Education, Nanjing 210096, China. [3] Nottingham Geospatial Institute, The University of Nottingham, Nottingham NG7 2TU, UK. [4] Global Geospatial Engineering Ltd./Sino-UK Geospatial Engineering Centre, Radford Bridge Road, Nottingham NG8 1NA, UK. [5] State Key Laboratory of Media Convergence Production Technology and Systems, Beijing 100031, China. [6] School of Transportation, Southeast University, Nanjing 210096, China.

Received: 30 September 2020 Accepted: 2 January 2021
Published online: 08 March 2021

References

Banville, S., Lachapelle, G., Ghoddousi-Fard, R., et al. (2019, September). Automated processing of low-cost GNSS receiver data. In *Proceedings of institute of navigation GNSS+ 2019 conference*.

Chen, B., Gao, C., Liu, Y., et al. (2019). Real-time precise point positioning with a Xiaomi MI 8 android smartphone. *Sensors, 19*(12), 2835.

de Bakker, P., van der Marel, H., & Tiberius, C. (2009). Geometry-free undifferenced, single and double differenced analysis of single frequency GPS. EGNOS and GIOVE-A/B measurements. *GPS Solutions, 13*(4), 305–314.
Fortunato, M., Critchley-Marrows, J., Siutkowska, M., et al. (2019). Enabling high accuracy dynamic applications in urban environments using PPP and RTK on android multi-frequency and multi-GNSS smartphones. In *2019 European navigation conference (ENC)* (pp. 1–9). IEEE.
Gao, H., & Groves, P. (2018). Environmental context detection for adaptive navigation using GNSS measurements from a smartphone. *Navigation: Journal of the Institute of Navigation, 65*(1), 99–116.
Gill, M., Bisnath, S., Aggrey, J., et al. (2017). Precise point positioning (PPP) using low-cost and ultra-low-cost GNSS receivers. In *Proceedings of the ION GNSS* (pp. 226–236).
Gu, S., Wang, Y., Zhao, Q., et al. (2020). BDS-3 differential code bias estimation with undifferenced uncombined model based on triple-frequency observation. *Journal of Geodesy, 94,* 45.
Guo, S., Cai, H., Meng, Y., et al. (2019). BDS-3 RNSS technical characteristics and service performance. *ActaGeodaetica et CartographicaSinica, 48*(7), 810–821. ((**In Chinese)**).
GSA. (2019). GSA GNSS Market Report Issue 6 (available at: www.gsa.europa.eu/system/files/reports/market_report_issue_6_v2.pdf. Accessed on August 10, 2020
IGS MGEX. (2020). http://mgex.igs.org/IGS_MGEX_Status_BDS.php. Accessed on August 17, 2020
Liu, J., Gao, K., Guo, W., et al. (2020). Role, path, and vision of "5G+ BDS/GNSS." *Satellite Navigation, 1*(1), 1–8.
Liu, W., Shi, X., Zhu, F., et al. (2019). Quality analysis of multi-GNSS raw observations and a velocity-aided positioning approach based on smartphones. *Advances in Space Research, 63*(8), 2358–2377.
Lu, M., Li, W., Yao, Z., et al. (2019). Overview of BDS III new signals. *Navigation, 66*(1), 19–35.
Lv, Y., Geng, T., Zhao, Q., et al. (2020). Initial assessment of BDS-3 preliminary system signal-in-space range error. *GPS Solutions, 24*(1), 16.
Meng, X., Roberts, G., Dodson, A., et al. (2004). Impact of GPS satellite and pseudolite geometry on structural deformation monitoring: analytical and empirical studies. *Journal of Geodesy, 77*(12), 809–822.
Niu, Z., Nie, P., Tao, L., et al. (2019). RTK with the assistance of an IMU-based pedestrian navigation algorithm for smartphones. *Sensors, 19*(14), 3228.
Odolinski, R., & Teunissen, P. (2019). An assessment of smartphone and low-cost multi-GNSS single-frequency RTK positioning for low, medium and high ionospheric disturbance periods. *Journal of Geodesy, 93*(5), 701–722.
Paziewski, J., Sieradzki, R., & Baryla, R. (2019). Signal characterization and assessment of code GNSS positioning with low-power consumption smartphones. *GPS Solutions, 23*(4), 98.
Reußner, N., & Wanninger, L. (2012). GLONASS inter-frequency code biases and PPP carrier-phase ambiguity resolution. *Journal of Geodesy, 86,* 139–148.
Riley, S., Landau, H., Gomez, V., et al. (2018). Positioning with android: GNSS observables. *GPS World, 29*(1), 18–34.
Sharawi, M., Akos, D., & Aloi, D. (2007). GPS C/N0 estimation in the presence of interference and limited quantization levels. *IEEE Transactions on Aerospace and Electronic Systems, 43*(1), 227–238.
Shi, J., Ouyang, C., Huang, Y., et al. (2020). Assessment of BDS-3 global positioning service: Ephemeris, SPP, PPP, RTK, and new signal. *GPS Solutions, 24*(3), 1–14.
Specht, C., Dabrowski, P., Pawelski, J., et al. (2019). Comparative analysis of positioning accuracy of GNSS receivers of Samsung Galaxy smartphones in marine dynamic measurements. *Advances in Space Research, 63*(9), 3018–3028.
Sun, W., Li, Y., & Duan, S. (2020). Xiaomi Mi 8 smartphone GNSS data quality analysis and single-frequency RTK positioning performance evaluation. In *IET radar, sonar & navigation*.
Takasu, T., & Yasuda, A. (2009). Development of the low-cost RTK-GPS receiver with an open source program package RTKLIB. In *International symposium on GPS/GNSS* (pp. 4–6). International Convention Center Jeju Korea.
Wang, C., Zhao, Q., Guo, J., et al. (2019a). The contribution of intersatellite links to BDS-3 orbit determination: Model refinement and comparisons. *Navigation, 66*(1), 71–82.
Wang, L., Li, Z., Zhao, J., et al. (2016). Smart device-supported BDS/GNSS real-time kinematic positioning for sub-meter-level accuracy in urban location-based services. *Sensors, 16*(12), 2201.
Wang, M., Wang, J., Dong, D., et al. (2019b). Performance of BDS-3: satellite visibility and dilution of precision. *GPS Solutions, 23*(2), 56.
Wang, Q., Jin, S., Yuan, L., et al. (2020). Estimation and analysis of BDS-3 differential code biases from MGEX observations. *Remote Sensing, 12*(1), 68.
Wanninger, L., & Heßelbarth, A. (2020). GNSS code and carrier phase observations of a Huawei P30 smartphone: quality assessment and centimeter-accurate positioning. *GPS Solutions, 24*(2), 64.
Xie, X., Fang, R., Geng, T., et al. (2018). Characterization of GNSS signals tracked by the iGMAS network considering recent BDS-3 satellites. *Remote Sensing, 10*(11), 1736.
Xie, X., Geng, T., Zhao, Q., et al. (2019). Precise orbit determination for BDS-3 satellites using satellite-ground and inter-satellite link observations. *GPS Solutions, 23*(2), 40.
Xia, Y., Pan, S., Gao, W., et al. (2020). Recurrent neural network based scenario recognition with multi-constellation GNSS measurements on a smartphone. *Measurement, 153,* 107420.
Yang, Y., Gao, W., Guo, S., et al. (2019). Introduction to BeiDou-3 navigation satellite system. *Navigation, 66*(1), 7–18.
Yang, Y., Mao, Y., & Sun, B. (2020). Basic performance and future developments of BeiDou global navigation satellite system. *Satellite Navigation, 1*(1), 1–8.
Zhang, K., Jiao, W., Wang, L., et al. (2019a). Smart-RTK: Multi-GNSS kinematic positioning approach on android smart devices with Doppler-smoothed-code filter and constant acceleration model. *Advances in Space Research, 64*(9), 1662–1674.
Zhang, X., Tao, X., Zhu, F., et al. (2018). Quality assessment of GNSS observations from an Android N smartphone and positioning performance analysis using time-differenced filtering approach. *GPS Solutions, 22*(3), 70.
Zhang, Y., Kubo, N., Chen, J., et al. (2020). Apparent clock and TGD biases between BDS-2 and BDS-3. *GPS Solutions, 24*(1), 27.
Zhang, Z., Li, B., Nie, L., et al. (2019b). Initial assessment of BeiDou-3 global navigation satellite system: signal quality, RTK and PPP. *GPS Solutions, 23*(4), 111.
Zhu, F., Tao, X., Liu, W., et al. (2019). Walker: Continuous and precise navigation by fusing GNSS and MEMS in smartphone chipsets for pedestrians. *Remote sensing, 11*(2), 139.

Publisher's Note